Dislocations in stripes and lattice Dirac fermions

Mesaroš, A.

Chapter 5

Dislocations and the Identity of Majorana Fermions

5.1 Introduction

As discussed in the introductory Chapter, the topological insulators (TI) [74, 81, 203] have gapless edge (2DTI) or surface (3DTI) states that are helical (spin direction is tied to propagation direction), topologically protected in the absence of time-reversal symmetry (TRS) breaking fields. Breaking TRS by a deposition of a magnetic (M) material can open an insulating energy gap in the edge states. Depositing a superconductor (S) on the edge or surface induces, via the proximity effect, a superconducting gap. Remarkably, the edge or surface can host Majorana bound states (MBS) at an STIM interface, where the gap "changes sign" from the M to the S type [204]. The situation where localized states are created at interfaces where the induced gap in the Dirac spectrum changes is familiar: in polyacetylene chains [29], the gap is opened by the Peierls distortion of the chain (the unit-cell is doubled), and this gap will "change sign" at a domain wall where the two different degenerate patterns of the Peierls distortion meet; in bilayer graphene [165], it was shown that the domain wall between two regions with opposite sign of applied electric potential also confines the Dirac particles. In topological insulators, the TRS of the original system ensures the special property that the bound states are Majorana fermions, meaning that the particle is its own anti-particle.

There is a strong interest to realize, observe and manipulate Majorana fermions, because of the non-Abelian statistics they possess [205], being the ba-

sis for topological quantum computation [206]. Majorana fermions have been argued to be present in the $\nu = 5/2$ fractional quantum Hall state [205, 207], in the $p-$wave superconductor Sr_2RuO_4 [208] and in topological insulator-superconductor junctions [204, 209, 210]. In the context of the $\nu = 5/2$ quantum Hall state, recent experiments have identified the charge of the $e/4$ quasiparticle modes [211, 212], and current efforts are focused on identifying their non-Abelian nature. However, in superconductors, Majorana fermions have proven much more elusive, since they are neutral. There has been a surge of suggestions for the identification of these modes, ranging from rather indirect tunneling experiments [213–215], to interference experiments [216, 217].

In this Chapter, we will describe crystal dislocations as probes of the Majorana states in topological insulators.

5.2 Dislocations and Majorana states: conductance symmetries

Here we identify the fundamental effect of dislocations on 2DTI edge states, and propose a simple interferometer for using them to probe neutral Majorana fermion states. This is a standard Aharonov-Bohm (AB) interferometer (cf. Fig. 5.1), where the presence of dislocations within the interferometer area causes a topological phase shift on the edge states due to the translational effect of the dislocation Burgers vector on the edge wavefunction. This AB effect (see also Section 2.2) is analogous to the effect of pierced magnetic flux [216, 217], except that it *preserves* TRS. The magnetic flux induces electrical current flow, the persistent current, in the ground state. Analogously, dislocations induce the TRS invariant counterpart, *dissipationless spin currents*. Spin currents are typically hard to observe, but appear to be useful for MBS detection. Dislocations in 3DTI have also been found to host interesting states [218, 219].

The STIM interface locally breaks TRS and particle-hole symmetry (PHS) [204, 209, 210], so that clear experimental signatures in the two-terminal AB interferometer are expected. For instance, asymmetries of the magnetoconductance

$$G(\phi) \neq G(-\phi), \tag{5.1}$$

where ϕ is the threading magnetic flux, are typically absent due to TRS. We find that the magnetoconductance remains *even* in the presence of MBS, due to the topological *helicity* symmetry (exchange of the left/right moving up/down spin, for the left/right moving down/up spin edge modes). But when dislocations are present (this is controlled by straining the bulk of the TI), a spin current is introduced in the interferometer which is sensitive to the helicity flip and therefore can detect the signatures of MBS. Most strikingly, the oscillations $\delta G(\phi)$ switch from *even* with period $\phi_0/2$ (ϕ_0 is the flux quantum hc/e) to *odd* oscillations with period ϕ_0 when dislocations enter the device and the MBS are coupled (see

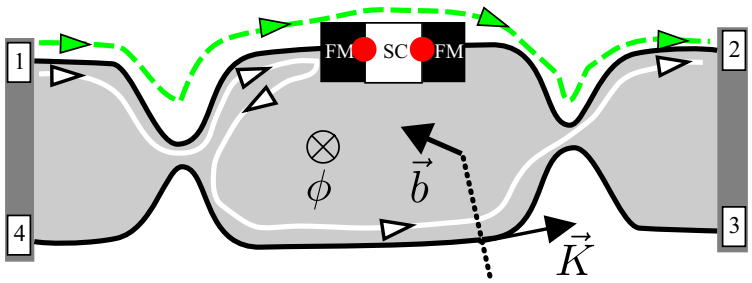

Figure 5.1: The experimental setup we propose aimed at observing neutral Majorana fermion bound states (MBS). Edge modes of the 2D topological insulator (TI, grey shaded area) traverse an interferometer, where at its upper arm there is a pair of superconductor (SC) - ferromagnet (FM) - topological insulator (TI) junctions, where the MBS (red dots) are present. Electrons circulating along the edges interact with the MBS. The 2D TI is threaded by 3D dislocation lines with a Burgers vector $\vec{b}$. The dislocation induces a translation on the half-plane of missing atoms (dotted line), causing a topological phase shift $\exp(i\vec{K}\cdot\vec{b})$, where $\vec{K}$ is the three-dimensional embedding of the edge state momentum K. The two simplest Feynman paths (white and dashed green (light grey)) contribute to Aharonov-Bohm oscillations in the two-terminal conductance, caused by the topological phase shift of the dislocations and/or the magnetic flux ϕ.

Fig. 5.1), while oscillations vanish in the absence of MBS at the STIM. We predict that the conductance satisfies the relation,

$$G(\phi, E, \phi_{\mathrm{d}}) = G(-\phi, -E, -\phi_{\mathrm{d}}) \tag{5.2}$$

(E incident electron energy, and ϕ_{d} the dislocation scattering topological phase), which allows the use of the topological effect of dislocations (ϕ_{d}) as a control parameter to bring out the signatures of the MBS. We further expect the rightful use of dislocation induced spin currents as novel TRS probes in the future. Given the experimental observation of 2D [83] and 3D [87,88,220] topological insulators, with dislocations being the most natural and abundant topological defects in crystals (controllable by shear stresses), it seems plausible that the proposed setup is experimentally possible, pending the STIM interface.

5.3 The proposed interferometer setup

Our interferometer is made up of a 2DTI (*e.g.* HgTe quantum well) (cf. Fig. 5.1) shaped by two point contacts, and we model it using the scattering matrix formalism, which should provide a correct description at low temperatures in the regime of coherent transport [221]. The edge segments comprising the interferometer support two *chiral* modes, one electron and one hole, traveling in both

directions with opposite spin. The Bogoliubov - de Gennes Hamiltonian describing the edge segments is,

$$\tau_3(v_F\hat{p}\,\sigma_3 + A_d + \tau_3\sigma_3 eA/\hbar c - E_F)\Psi = E\Psi, \tag{5.3}$$

where $\hat{p} \equiv -i\hbar\partial/\partial x$, E_F the Fermi energy, v_F the Fermi velocity, and A the magnetic vector potential. The four-component spinor is $\Psi = (\Psi_{e\uparrow}, \Psi_{e\downarrow}, \Psi_{h\uparrow}, \Psi_{h\downarrow})^T$ while the τ matrices mix the electron and hole parts of the wavefunction, and σ the spin components.

The effect of dislocations is contained in the potential A_d of Eq. (5.3). It encodes for the AB effect:

$$\exp\left(i \oint A_d\, dx\right) = \exp\left(i2\pi\phi_{\rm d}\right), \tag{5.4}$$

with pseudo-flux $\phi_{\rm d}$ stemming from the topological effect of the dislocation on the wavefunctions on the edge as they circulate the interferometer. As also previously introduced in Chapter 2, it is well known that this effect is described by a *translation* by the Burgers vector $\vec{b}$ on traversal of electron around the dislocation core line [12]. The translation operator $\exp\left(i\vec{K}\cdot\vec{b}\right) \equiv \exp\left(i2\pi\phi_{\rm d}\right)$ is determined by the Burgers vector $\vec{b}$ of the dislocation line threading the TI inside the ring-shaped area of the interferometer. The $\vec{b}$ is three-dimensional and could be due to any type (edge, screw or mixed) of dislocations. The wavevector $\vec{K}$ is the three-dimensional embedding of the edge wavefunction wavevector K [74] (see Fig. 5.1). The dislocation effects discussed in this Letter depend on one-dimensional momentum K on the edge being non-zero; such 2DTI variety is not yet realized, but it is expected that such edge states are present in Heusler alloys [222]. Dislocations preserve time reversal and particle hole (PHS) symmetries, represented by $T = i\sigma_2 C$ and $\Xi = \tau_2\sigma_2 C$, respectively, with C the complex conjugation, and they are distinct from ordinary disorder due to their intrinsic gauge symmetry.

5.3.1 Scattering formalism

The Hamiltonian of Eq. (5.3) determines the energy dependent wavevector of the left (spin down on upper edge), and right (spin up on upper edge), moving electron, as well as their time reversed hole pairs. The point contacts, the two halves of the upper ring arm, the coupled MBS between the two upper arm halves, and the lower ring arm are all described by single scattering points with corresponding matrices ($S_{\rm scatt}$). Each matrix $S_{\rm scatt}$ connects the amplitudes ($\boldsymbol{O}_L$ and $\boldsymbol{O}_R$) of the modes *outgoing* to the left/right (L/R) side, to the amplitudes ($\boldsymbol{I}_L$ and $\boldsymbol{I}_R$) of the modes *incoming* from the left/right side, with respect to that particular scatterer. Using $O^T = (\boldsymbol{O}_L, \boldsymbol{O}_R)^T = (o^L_{e\downarrow}, o^L_{h\uparrow}, o^R_{e\uparrow}, o^R_{h\downarrow})^T$ and $I^T = (\boldsymbol{I}_L, \boldsymbol{I}_R)^T = (i^L_{e\uparrow}, i^L_{h\downarrow}, i^R_{e\downarrow}, i^R_{h\uparrow})^T$ we formally have $O = S_{\rm scatt} I$. On the lower

edge, spin directions $\downarrow, \uparrow$ are reversed, because their directions are opposite due to chirality. The scattering matrices have a block structure

$$S_{\text{scatt}} = \begin{pmatrix} r & t \\ t' & r' \end{pmatrix}, \tag{5.5}$$

representing reflection (r, r') and transmission (t, t'), where each block has electron/hole components:

$$t = \begin{pmatrix} t^{\text{ee}} & t^{\text{he}} \\ t^{\text{he}} & t^{\text{hh}} \end{pmatrix}. \tag{5.6}$$

When TRS is obeyed, backscattering is forbidden in the single-particle formalism, i.e. $r = r' = 0$ [223], because $T^2 = -1$. We compute the total scattering matrix S for the four leads (labeled from 1 to 4 in Fig. 5.1), determining the conductance of the device according to the Landauer-Büttiker quantum transport formalism.

Particle conservation is enforced by $S^\dagger S = \mathbb{1}$. For scattering matrices connecting two edge segments, TRS demands

$$S_{\text{scatt}}(\phi) = -\alpha_3 S_{\text{scatt}}(-\phi)^T \alpha_3, \tag{5.7}$$

and PHS is obeyed when

$$S_{\text{scatt}}(E) = \beta_1 S_{\text{scatt}}(-E) \beta_1, \tag{5.8}$$

where α and β are Pauli matrices acting on the L/R and e/h indices of S_{scatt}, respectively. For scattering involving all four edges (like in S) one should only replace α by $\alpha \otimes \alpha'$, where α' matrices exchange the two leads on the same side (i.e. 1 and 4, or 2 and 3). The scattering caused by the coupling to, and propagation through the two MBS in the upper arm is given by the scattering matrix S_{MBS} found in Ref. [210]. It is determined by two energy scales, the coupling between the two MBS E_M, and the coupling of edge states to the MBS Γ. Length is measured in units of the ring circumference L, ϕ in units of the flux quantum $\phi_0 = hc/e$, and energy in units of $\hbar v_F/L$. We consider the scattering mechanisms as follows:

(a) Propagation in the lower arm S_{low} is determined by nonzero elements:

$$t^{ee}_{\text{low}} = \exp\left[il_d(E + 2\pi\phi_{\text{d}} - 2\pi\phi)\right] \tag{5.9}$$

$$t^{hh}_{\text{low}} = \exp\left[il_d(E - 2\pi\phi_{\text{d}} + 2\pi\phi)\right], \tag{5.10}$$

where l_u is the length of the lower arm;

(b) In the upper arm segments $S_{\text{up}} = S^T_{\text{low}}$, with l_d replaced by l_{u1}, and l_{u2} in the two segments, respectively;

(c) Without loss of generality we take the point contact scattering matrix S_{PC} to be real and satisfying the TRS and PHS symmetries (edge segments are

ordered as $(1,4)$ on the left and $(2,3)$ on right, cf. Fig. 5.1):

$$S_{\rm PC} = \begin{pmatrix} 0 & a & b & b' \\ a & 0 & -b' & b \\ b & b' & 0 & -a \\ -b' & b & -a & 0 \end{pmatrix} \otimes \beta_0, \tag{5.11}$$

with $\beta_0 = \mathbb{1}$, and $a^2 + b^2 + b'^2 = 1$. Parameter a describes the coupling of the ring-shaped middle of the interferometer to the leads ($a = 0$ corresponds to an isolated ring with $G = 0$). The ratio $\epsilon \equiv b/b'$ measures the asymmetry of current injected into the lower and upper ring arms ($\epsilon = 0$ corresponds to all particles from lead 1 being injected into the lower arm, and all from lead 4 into the upper arm). Following Refs. [224,225], in the present single particle scattering we attain the conductance of the charge-conductor/spin-insulator (CI) state, by choosing $a = 1/\sqrt{3}$, $\epsilon = 1$, being in the regime of Luttinger liquid coupling $g_c > 2$. In the realistic case of intermediate $0 < a < 1$, the dependence on a and ϵ is weak, so in the following we present results for CI point contacts.

The conductance is given by

$$G = e^2/h \sum_{\substack{i=1,4 \\ j=2,3}} \left(|S_{ij}^{ee}|^2 - |S_{ij}^{he}|^2 \right), \tag{5.12}$$

where i, j label the leads, and holes contribute opposite charge current from electrons. The zero temperature conductance at zero voltage corresponds to taking $E = 0$ in G, while at low enough temperature and voltage difference, E is given by the external voltage ($E = eV_1$). We consider $E_F = 0$, and fix $l_{u1} = l_{u2} = l_d/2 = L/2$, while the results are insensitive to the asymmetry in l_{u1} and l_{u2}. The point contact parameters a, ϵ are set to be the same in the left and right contact, since results are insensitive to this asymmetry too.

The symmetry expressed in Eq. 5.2 is most revealing since it controls the behavior of the conductance $G(\phi, E)$, given the changes in the net Burgers vector d. It represents the invariance of the edge states to switching the spin orientation of left and right moving carriers (This spin orientation is set by the sign of the spin-orbit coupling term in the bulk.) For the scattering on the edge, this switch is represented by conjugation C, i.e. the combined time-reversal and spin-flip operation. In this case, it follows that:

$$S_{\rm scatt}(E) = S_{\rm scatt}(-E)^*, \tag{5.13}$$

and non-trivially for the case of S_{MBS}, this property holds because

$$H_M^* = -H_M. \tag{5.14}$$

The two-level Hamiltonian H_M fundamentally obeys the relation because the Majorana fields are real, i.e. $\gamma_a^\dagger = \gamma_a$. We expect the spin-flip symmetry to be robust in absence of Zeeman type coupling to out-of-plane magnetic fields.

5.3.2 Detecting Majoranas with dislocations

We first consider the effect of dislocations on a trivial interferometer, one without a STIM interface. The presence of $\phi_{\rm d} \neq 0$ introduces a deviation from evenness in $G(E)$, as the symmetry $G(E, \phi_{\rm d}) = G(-E, -\phi_{\rm d})$ suggests. The magnetoconductance $G(\phi) = G(-\phi)$ stays even, protected by TRS in a two terminal measurement. However, the nature of the $G(\phi)$ oscillations switches from dominantly universal conductance fluctuations (UCF), i.e. period ϕ_0, to a dominantly period $\phi_0/2$ nature, when dislocation is introduced.

Secondly, we introduce the STIM interface into the upper arm of the interferometer (cf. Fig. 5.1). If there are *no* MBS forming, the STIM is a segment of gapped edge states with a TRS violation. The absence of MBS is modeled by setting $\Gamma = 0$ (decoupling from the edges). In this case, the magnetoconductance oscillations $\delta G(\phi)$ vanish. The dislocations influence the oscillations, and $G(E, \phi_{\rm d}) = f(E - \phi_{\rm d})$, with

$$f(x) = b'^2(1 - a^4)\frac{(1 + a^2)(1 + \epsilon^2) + 4a\epsilon\cos(x/2)}{1 + a^8 + 2a^4\cos(2x)}, \tag{5.15}$$

which shows clearly that the asymmetry of $G(E)$ is controlled by the dislocations. The effect persists in the limit where the central ring is decoupled from the leads, i.e. when $a = 0$, and also then $G = 0$: the spectrum of the isolated ring is given by the solutions of $\cos(2E) = \cos(\pi\phi_{\rm d})$, and shows the spectrum (a)symmetries

$$\{E_n(\phi_{\rm d})\} \neq -\{E_n(\phi_{\rm d})\} \tag{5.16}$$

$$\{E_n(\phi_{\rm d})\} = -\{E_n(-\phi_{\rm d})\}. \tag{5.17}$$

Note that in this geometry of the isolated ring it becomes obvious that the dislocation effect, just as the AB magnetic flux effect, can be literally assigned to a boundary condition at the point where the periodicity of the one-dimensional system (the ring "cut open") is imposed, with the important distinction that dislocations do not break TRS. In this spirit we introduced the dislocation gauge field in Eq. (5.4).

The general asymmetry features in $G(E)$ due to dislocations persist when MBS are added, and new signature effects appear in the magnetoconductance as dislocations are manipulated. The dependence $G(E)$ shows oscillatory behavior, with resonances at $\pm E_M$, shown in Fig. 5.2(a). In Fig. 5.2(b), we provide a summary of the dislocation effect on the behavior of $G(E)$. Introduction of nonzero dislocation phase causes a large asymmetry and the effect persists for all values of E_M. If the flux ϕ is present, $G(E)$ becomes asymmetric at any value of $\phi_{\rm d}$, and more strongly as E_M increases (note that when MBS are absent, there is no dependence on ϕ). The last observation was made also for a more complicated hypothetical interferometer in Ref. [217].

Fig. 5.3 presents the characteristic influence of dislocations and Majorana states on the magnetoconductance at zero energy (*i.e.* zero voltage at low temperatures). As announced, even though TRS is broken by the MBS scattering, a

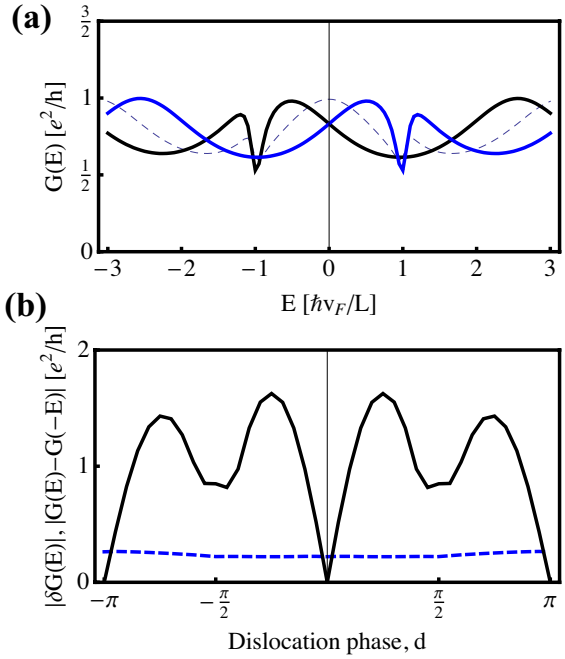

Figure 5.2: The properties of energy (external voltage) dependent conductance, as function of dislocation, with $E_M = 1$. (a) Example curves: no dislocation (dashed thin black line); dislocation phase $\phi_{\rm d} = 0.1$ (thick black); and $\phi_{\rm d} = -0.1$ (thick light grey (blue)). Note the resonances at $\pm E_M = \pm 1$, and the asymmetry induced by the dislocation. (b) The asymmetry of the $G(E)$ curves (full black line), calculated as $Max_E[G(E) - G(-E)]$ on the interval $E \in [0, 3]$, as function of dislocation phase $\phi_{\rm d}$. (The asymmetry reaches 2 for purely odd $G \sim \sin(E)$). The dashed grey (blue) line shows the amplitude of oscillations in $G(E)$ around the mean value. The curves are robust to changes in E_M.

resulting non-even $G(\phi)$ is observed only in the presence of dislocations. Namely, $\delta G(\phi)$ has two prominent Fourier components, and both have *definite parity*: the UCF in the form of $\sin(\phi)$ (period ϕ_0), and the harmonic $\cos(2\phi)$ (period $\phi_0/2$). When $E_M = 0$ (MBS decoupled from each other), the UCF vanish. However, when $E_M \neq 0$, dislocations show a clear signature: in their presence, as E_M/Γ increases, the harmonic is suppressed in favor of the UCF, and therefore simultaneously the transformation from even to odd $G(\phi)$ is observed! If $E_M > \Gamma$, a small value of $\phi_{\rm d}$ (e.g. 0.05) already causes a linear $G(\phi)$ up to $|\phi| \lesssim 1/4$ (cf. Fig. 5.3).

In the last paragraph of this subsection, we present the intuitive way of describing how the UCF, period ϕ_0, oscillations arise (these are normal Aharonov-

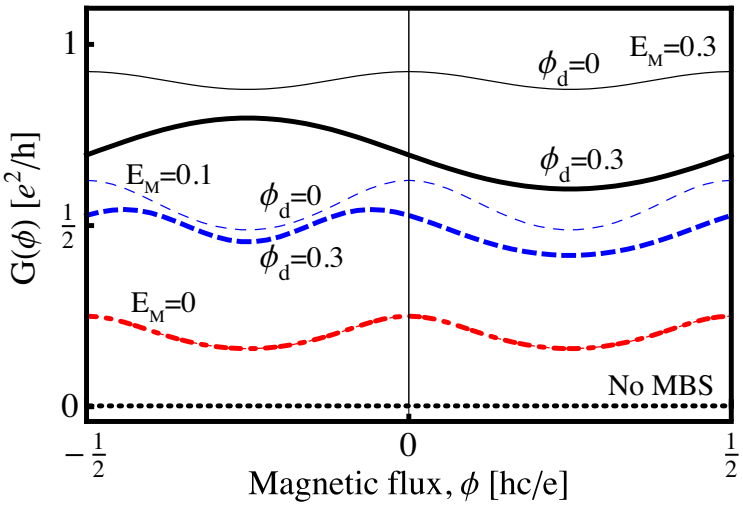

Figure 5.3: Magnetoconductance $G(\phi)$ at zero energy (voltage) as function of dislocations and Majorana couplings. In absence of MBS, $G(\phi)$ vanishes (dotted black line). The dash-dotted (red), dashed (blue) and full (black) curves correspond to three regimes of MBS coupling $E_M = 0, 0.1, 0.3$, respectively, with respect to MBS-edge coupling $\Gamma = 0.1$ (units $\hbar v_F/L$). The case of absence ($\phi_\mathrm{d} = 0$) or presence ($\phi_\mathrm{d} = 0.3$) of dislocations is distinguished by thin and thick lines, respectively, for each E_M value. Without dislocations, the result $\delta G \sim \cos(2\phi)$ is robust to interferometer parameter changes. The presence of dislocations affects *only* the cases of coupled MBS, $E_M \neq 0$, by suppressing the $\phi_0/2$ harmonic in $G(\phi)$ in favor of the ϕ_0, which is always *odd*, i.e. $\sin(\phi)$.

Bohm oscillations). Starting from the limit of decoupled interferometer ($a = 0$), one can treat the coupling to the leads a as a perturbation. Consider the Feynman path interpretation of the electron amplitude: When the incoming electron is in lead 1, and it leaves through leads 2 or 3, there is a path represented by dashed green line in Fig. 5.1. Its amplitude A_0 is independent of value of a, because the electron does not switch between ring arms. A second electron path exists, represented by the white full line in Fig. 5.1, whose amplitude A_1 is linear in a, because it switches ring arms only once, after backscattering in the upper. The interference of these two paths gives a non-vanishing oscillatory contribution to $G(\phi, \phi_\mathrm{d})$, which is linear in a. The two Feynman paths in Fig. 5.1 have to be *subtracted*, because they contribute through $G_A = A_0^* A_1 + A_1^* A_0$, which results in precisely one traversal around the ring of the interferometer. Upon one traversal the accumulated magnetic topological phase is ϕ_0, a fact that is encoded explicitly in Eq. (5.10). In a similar fashion, one can see that considering two longer paths, which have an additional full traversal with respect to the "white" and

"green" paths, their interference contributes to the $\phi_0/2$ oscillations.

5.4 Conclusions

We demonstrated the usefulness of topological lattice defects in observing and manipulating neutral Majorana fermions in TIs. In particular, we showed that the oscillatory features of the magnetoconductance at zero energy, carry clear signatures of the interplay between MBS and dislocations. Such signatures are due to spin currents that are induced on the TI edges because of the very presence of dislocations in the system. In addition, we showed that in the presence of dislocations, the conductance satisfies the enhanced symmetry of Eq. 5.2, a direct consequence of the topological symmetry of the parent insulator.